CHAPTER 3

MATERIALS, METHODOLOGY AND CHARACTERIZATION TECHNIQUES

3.1 Overview

This chapter outlines the experimental details involved in synthesizing the materials used in this research, along with the fundamental methods and protocols. Each section contains a different theme mainly the basic materials and different characterization techniques used in this research.

3.2 Materials and methods

This section describes the materials utilized in this work, including the sources. This section also labels the synthesis techniques of the matrix, reinforcement, and its composites.

3.2.1 Synthesis of 3-mol% yttrium stabilized zirconia (3Y-TZP)

The raw materials used for the synthesis of 3-mol% yttrium-stabilized zirconia were zirconium oxychloride octahydrate ($ZrOCl_2.8H_2O$), yttrium oxide (Y_2O_3), and nitric acid (HNO_3). All raw materials were purchased from Sigma Aldrich, Germany, with 99.98 % purity. Fig.3.1 represents the flow chart for the 3Y-TZP synthesis. Initially, zirconium nitrate and yttrium nitrate solution were prepared and mixed stoichiometrically to form a composite nitrate solution. Urea was added as a fuel in the composite nitrate solution in a ratio of two moles per mole of the metal ion. After 15 minutes of stirring, this solution was formed into a homogenized transparent solution. The clear solution was then placed in a muffle furnace set to 500°C, where it was burned to ashes through self-propagating combustion (Biswas *et al.*, 2011). This fluffy white powder was then crushed using a mortar and pestle and calcined for 4 hrs at 500°C with a 2°C/minute heating rate in an oxidizing environment. All of these calcined samples were ultimately reground and run through sieves with a mesh size of 250 before being further characterized.

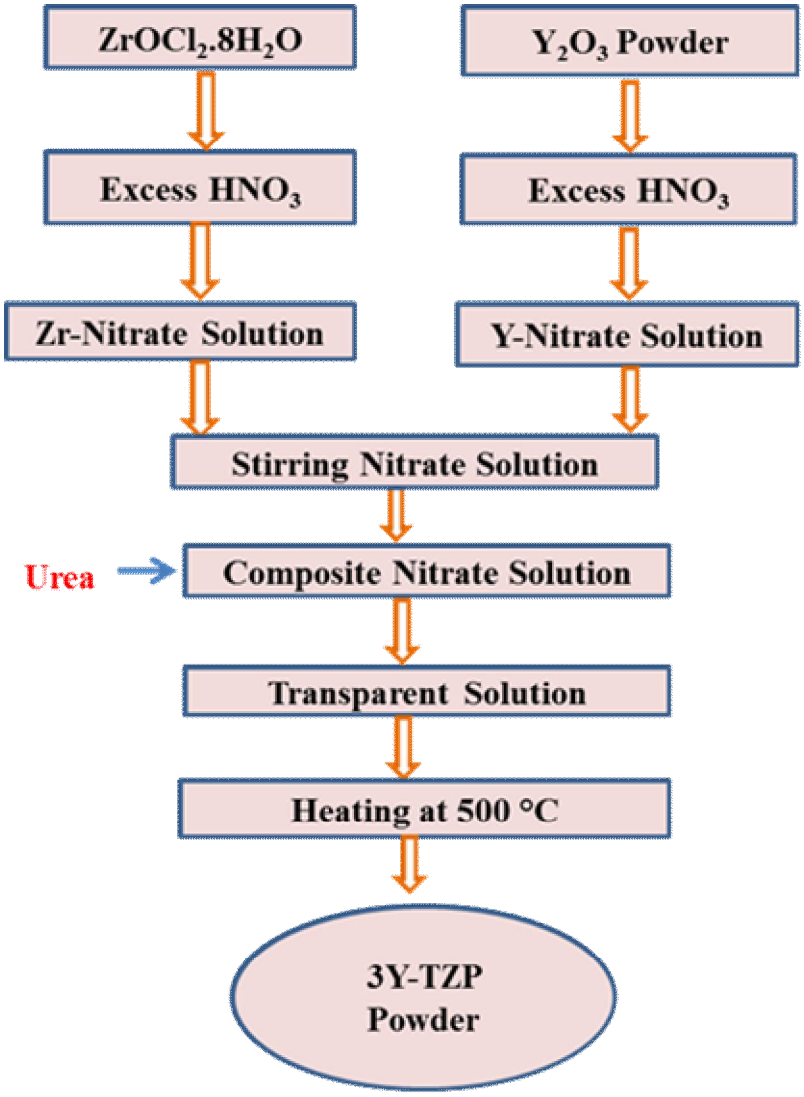

Fig. 3.1 Flow chart represents the 3Y-TZP synthesis method (Biswas *et al.*, 2011).

3.2.2 Synthesis of 8-mol% magnesia stabilized zirconia (8Mg-PSZ)

The chemical ingredients required for the preparation of 8-mol% magnesia partially stabilized zirconia (8Mg-PSZ) were zirconium oxychloride octahydrate ($ZrOCl_2.8H_2O$), nitric acid (HNO_3), Mg-nitrate hexahydrate [$Mg(NO_3)_2.6H_2O$], and urea (NH_2CONH_2). All raw ingredients with 99.98% purity were sourced from Sigma Aldrich in Germany. Fig.3.2. represents the flow chart for the 8Mg-PSZ synthesis. First, zirconium nitrate was prepared by mixing $ZrOCl_2.8H_2O$ into an HNO_3 solution. Then, a composite solution was prepared with zirconium nitrate and Mg-nitrate by stoichiometrically mixing the ingredients and continuing

stirring. In this method, urea was used as a fuel for a combustion reaction. Then, the composite solution was aged at 80-100°C until solvent evaporation was completed. Then, an auto-combustion reaction took place and converted it into a fluffy ash. After crushing this fluffy powder, it was put in the muffle furnace at 800°C for 4 hrs at with a 2°C/minute heating rate in an oxidizing environment for calcination. For further characterization, the calcined powder was ground again and passed through sieves (Lu *et al.*, 2022).

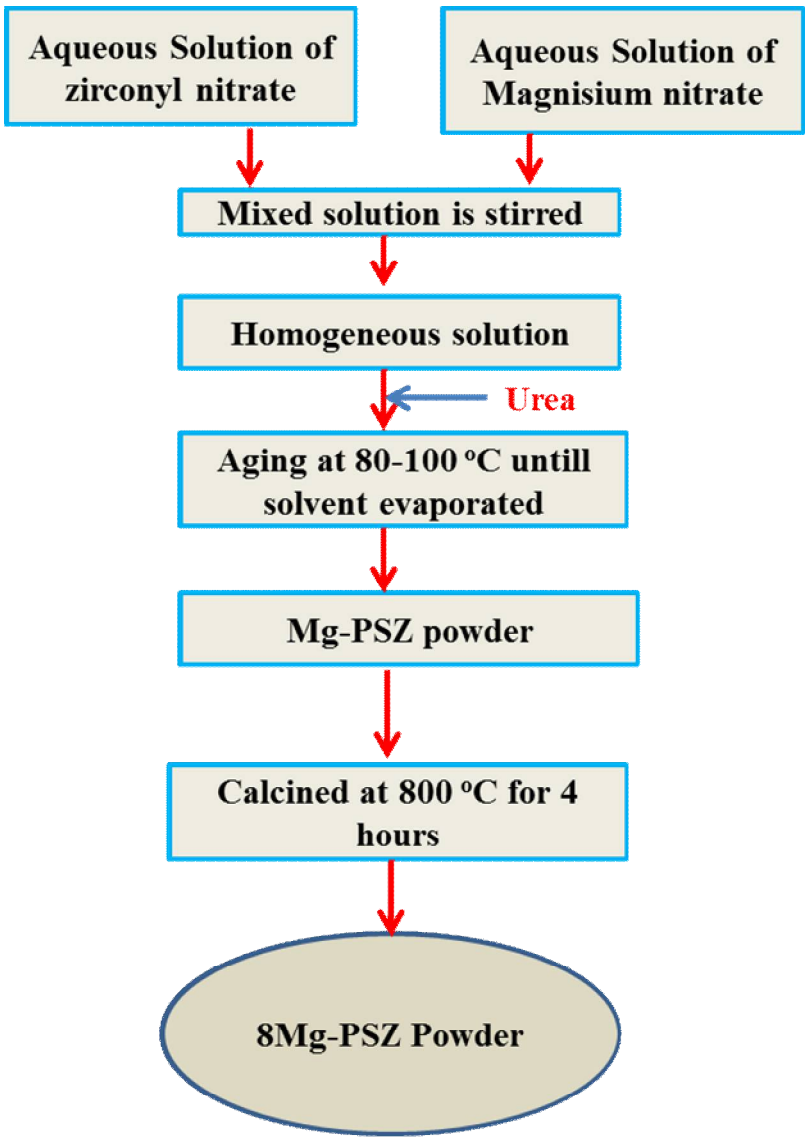

Fig. 3.2 Flow chart represents the 8Mg-PSZ synthesis method (Lu *et al.*, 2022).

3.2.3 Synthesis of 30-mol% zirconia toughened alumina (ZTA)

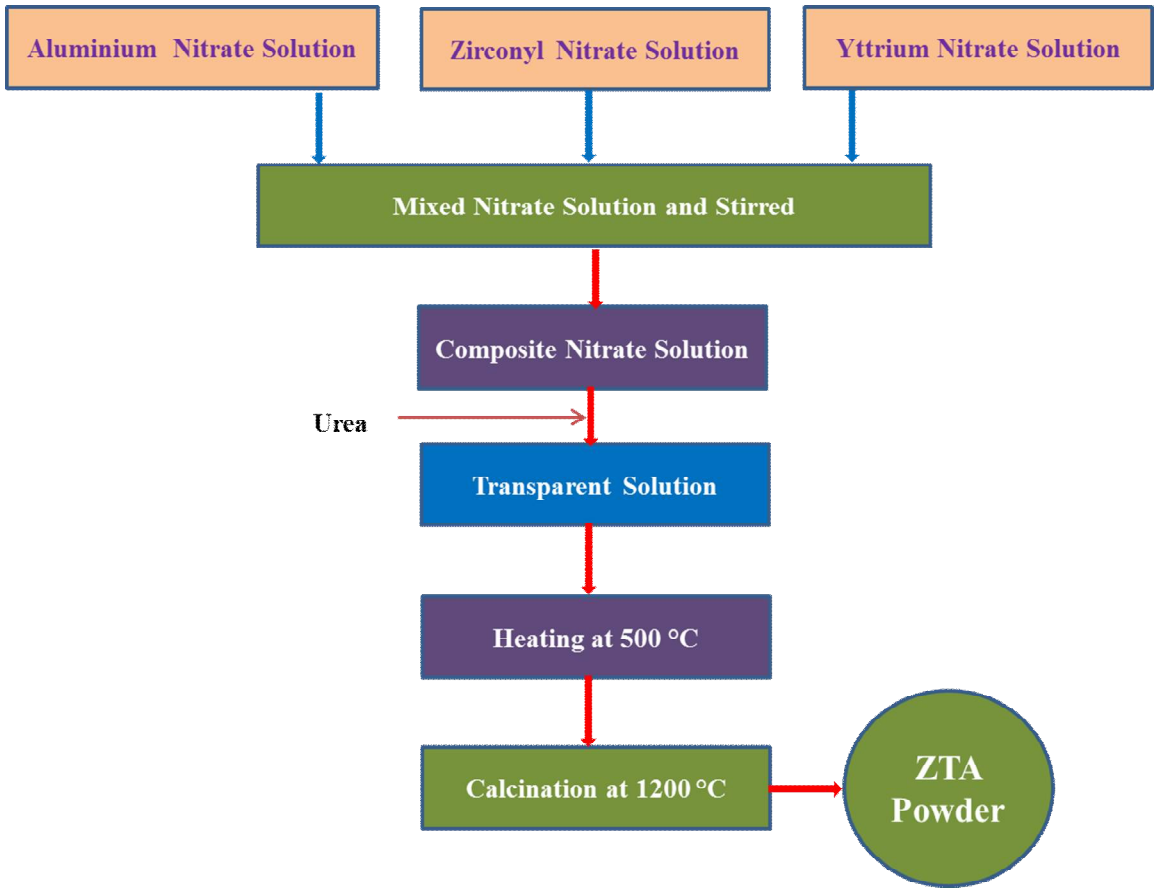

Fig. 3.3 Flow chart represents the ZTA synthesis method (Aruna *et al.*, 2004).

The ZTA ceramic (30% 3Y-TZP and 70% Al_2O_3) was made through the sol-gel auto-combustion route. The starting precursors, aluminum nitrate nonahydrate ($Al(NO_3)_3.9H_2O$), zirconium oxychloride hexahydrate ($ZrOCl_2.8H_2O$), nitric acid (HNO_3), and yttrium oxide (Y_2O_3) with a purity of 99.98% sourced from Sigma Aldrich (Germany) were taken. Fig.3.3 represents the flow chart for the ZTA synthesis. Initially, $ZrO(NO_3)_2.6H_2O$ and $Y(NO_3)_3.6H_2O$ were prepared by dissolving $ZrOCl_2.8H_2O$ and Y_2O_3 powder in excess HNO_3, respectively. The solutions of ($ZrO(NO_3)_2.6H_2O$ and $Y(NO_3)_3.6H_2O$) nitrates were combined in a specific ratio to yield the final 3 mol% yttria and 97 mol% zirconia powder (3Y-TZP). Then, the mixed solution was added with ($Al(NO_3)_3.9H_2O$) solution in an appropriate ratio to prepare ZTA ceramics. After that, these nitrate solutions were mixed stoichiometrically to

form a composite nitrate solution. Two moles of urea were added as fuel to each mole of metal ion in the composite nitrate solution. This solution formed a homogenized, translucent solution after 15 minutes of stirring. After that, the clear solution was put in a muffle furnace that was heated to 500°C, where self-propagating combustion burned it to ashes (Aruna *et al.*, 2004). Following a mortar and pestle crushing of this fluffy white powder, it was calcined for 4 hrs at 1200°C with a heating rate of two degrees Celsius per minute in an oxidizing atmosphere. Before being further examined, all of these calcined samples were eventually reground and passed through 250 mesh sieves.

3.2.4 Synthesis of 13-93 bioactive glass (BG)

13-93 BG composed of 53% SiO_2, 6% Na_2O, 12% K_2O, 4% P_2O_5, 6% MgO, and 20% CaO (wt%) was synthesized by the sol-gel method. These oxide precursors were obtained from tetraethyl orthosilicate (TEOS), sodium nitrate ($NaNO_3$), potassium nitrate (KNO_3), triethyl phosphate (TEP), magnesium nitrate hexahydrate ($Mg(NO_3)_2.6H_2O$), and calcium nitrate tetrahydrate ($Ca(NO_3)_2.4H_2O$), respectively. All raw materials were supplied by Sigma Aldrich Germany, with 99.98 % purity. Fig.3.4 flow chart represents the 13-93 bio-glass synthesis by sol-gel methods. Firstly, TEOS was added into 0.1 N HNO_3 aqueous solutions for hydrolysis and condensation. Subsequently, stoichiometrically TEP, $Ca(NO_3)_2.4H_2O$, $Mg(NO_3)_2.6H_2O$, $NaNO_3$, and KNO_3 were added at room temperature. Each precursor was mixed under continuous stirring and made a transparent solution. After vigorous stirring for 45 minutes, transparent sols were obtained. To facilitate the polycondensation reaction and gel formation, the clear sol was aged at room temperature. The prepared gels were dried after putting it in an oven at 75°C for 24 hrs. The calcination of dried gels was done at 600°C for 4 hrs to make the bioactive glass powder (Yadav *et al.*, 2020).

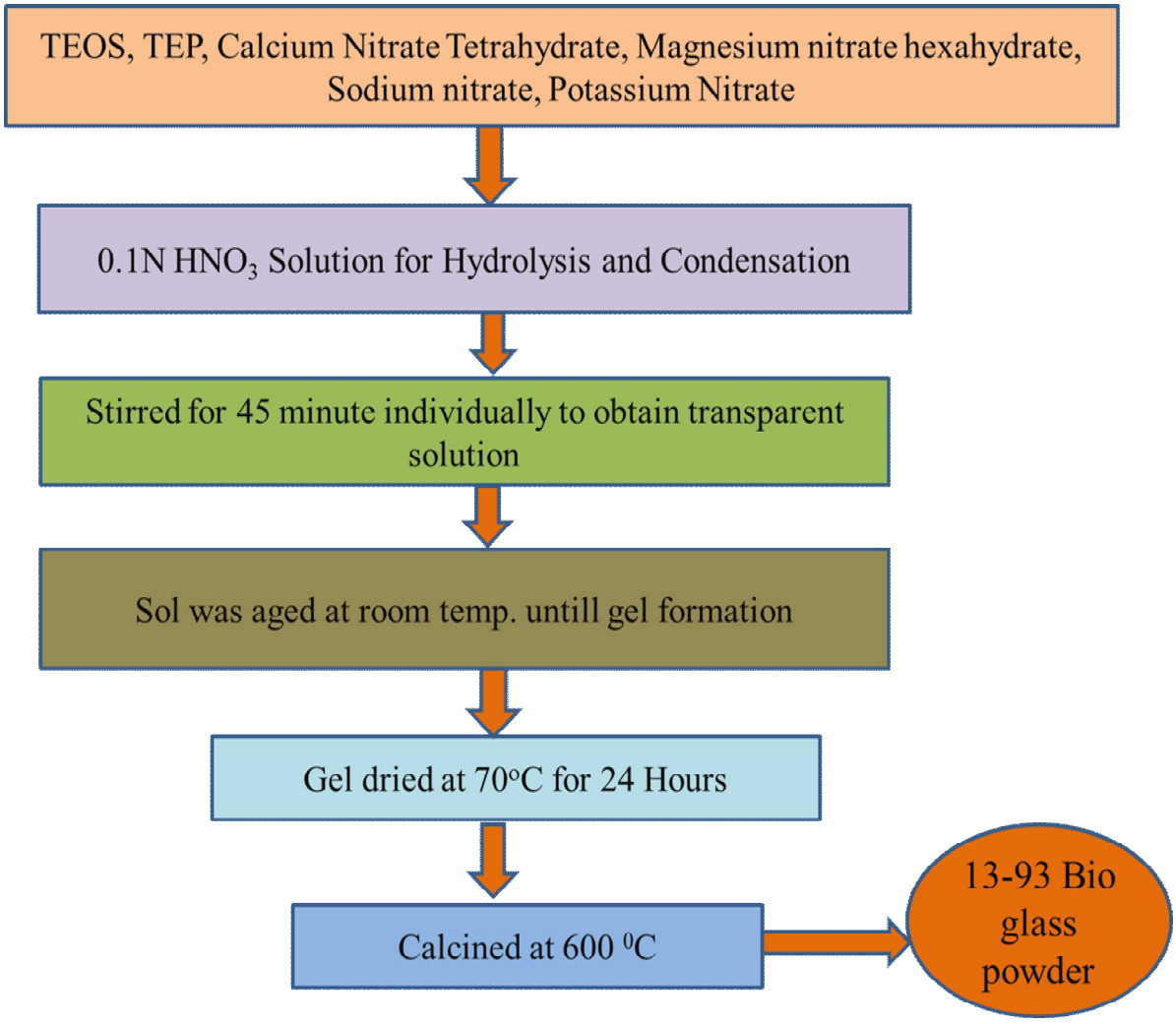

Fig. 3.4 Flow chart of synthesis 13-93 bio-glass by sol-gel method.

3.2.5 Synthesis of 3Y-TZP/13-93 BG biocomposites

The 3Y-TZP/13-93 BG composites were prepared by mixing synthesized materials in powder form in different weight proportions. The variations of compositions and sample identification are given in Table 3.1. The powders of 3Y-TZP and 13-93 BG were mixed in wet condition by a ball mill at 500 rpm for 2 hrs using an alumina ball of 5 mm diameter as grinding media. The mixture of biocomposite materials was finely powdered and then dried at 120°C for 12 hrs.

Table 3.1 Sample identification and different compositions of 3Y-TZP/13-93 BG biocomposite materials.

S. No	Sample Code	3Y-TZP (wt %)	13-93 BG (wt %)
1.	ZBG0	100	0
2.	ZBG5	95	5
3.	ZBG10	90	10
4.	ZBG15	85	15
5.	ZBG25	75	25

3.2.6. Synthesis of 8Mg-PSZ/13-93 BG biocomposites

The composites were made by combining prepared powders in various weight ratios. The different compositional changes and sample recognition are listed in Table 3.2. The 8Mg-PSZ and 13-93 BG powders were combined in a ball mill under wet conditions for 2 hrs at 500 rpm using an Al_2O_3 ball with a 5 mm diameter as the grinding media. The composite material mixture was finely pulverized and dried at 120°C for 12 hrs.

Table 3.2 Sample code and different compositions of 8Mg-PSZ/13-93 BG biocomposite materials.

S. No.	Sample Code	8Mg-PSZ (Wt%)	13-93BG (Wt%)
1.	MBG0	100	0
2.	MBG5	95	5
3.	MBG10	90	10
4.	MBG15	85	15
5.	MBG25	75	25

3.2.7. Synthesis of ZTA/13-93 BG biocomposites

The ZTA-BG composites were prepared by mixing both precursors ZTA and 13-93 BG, according to Table 3.3**.** The mixing of precursors was done in a ball mill with wet conditions for 2 hrs at 500 rpm. The grinding medium was an Al_2O_3 ball (5 mm diameter). Subsequently, the mixture was finely ground and dried at 120°C for 12 hrs.

Table 3.3 Sample identification and different compositions of ZTA/13-93 BG biocomposite materials.

S. No.	Sample Code	ZTA (Wt%)	13-93 BG (Wt%)
1.	ABG0	100	0
2.	ABG5	95	5
3.	ABG10	90	10
4.	ABG15	85	15
5.	ABG25	75	25

3.2.8 Granulation and pellet processing

The composite powders were obtained and uniformly combined in an agate mortar with a pestle. Next, the powder was evenly blended with 3% polyvinyl alcohol (PVA) until a fine consistency was achieved. The resulting fine powder was then compressed at 200 MPa to form pellets using a hydraulic press and a die with the required dimensions. The produced pellets are subsequently put into the furnace for sintering.

3.2.9 Sintering

Sintering is the method of heating a material to modify its microstructure, densify it, and form crystals. Sintering of the materials was carried out in numerous steps of thermal heating. The sample was heated from 1150 to 1350ºC at a rate of 3ºC/min and maintained for 4 hrs to completely densify. The pellets were cooled to room temperature at a rate of 3ºC per minute. The following section describes the further characterization procedures that were used to investigate the phase identification, densification, microstructure, mechanical and biological properties of pellets.

3.3 Materials characterization techniques

The important methods utilized to characterize the samples are explained in the following sections. The fundamental ideas underlying each technique will be briefly presented, with any relevant extra information supplied in the appendices.

3.3.1 Particle size analysis

According to Fig. 3.5, the particle size is determined by assessing the degree of incident laser scattering after colliding with each individual particle. The zetasizer system determines the particle size by determining the Brownian motion of the particles in a sample using DLS and then rendering a size from this using popular theories. Brownian motion is defined as the random movement of particles suspended in a liquid phase due to bombardment by surrounding molecules. Because the particles travel randomly, their movement speed can be used to determine the particle size. Smaller particles travel or diffuse faster than larger particles. The more the movement is intended for the smaller particle size, the less the movement indicates the larger particle size when the particle's position is examined in relation to time (Raja *et al.*, 2021). The measurement is conducted to find the particle size of all the calcined powders.

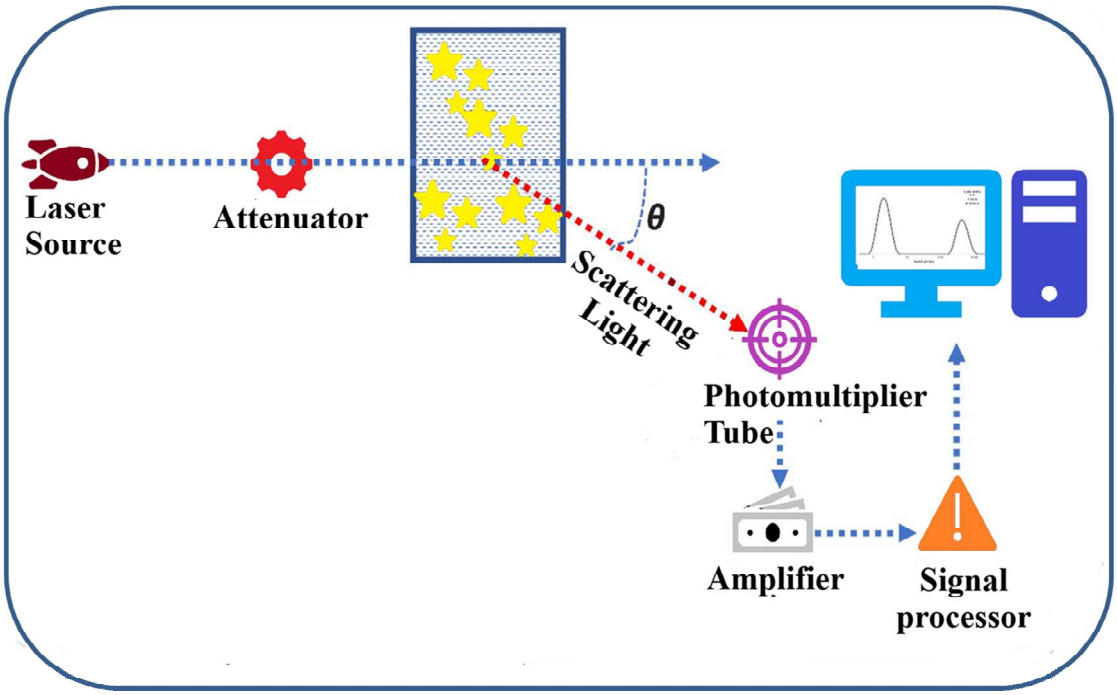

Fig. 3.5 Schematic representation of dynamic light scattering-based particle size analyzer.

3.3.2 X-ray diffraction analysis

The X-ray diffraction (XRD) technology is an important, non-contacting, and non-destructive approach to determine the crystalline phases and other structural properties. The XRD pattern can be used to assess atomic structures in qualitative as well as quantitative terms. Most of the physical attributes of the materials are sensitive to the structural requirements (atomic locations, crystallite size, shape, orientation, etc.), so it becomes critical to analyze the material using the XRD pattern. Fig. 3.6 represents the schematic basic scheme of an X-ray diffraction experiment. An incident X-ray beam enters the crystal and the diffracted rays produce a diffraction pattern (diffraction spots), which are recorded on a detector.

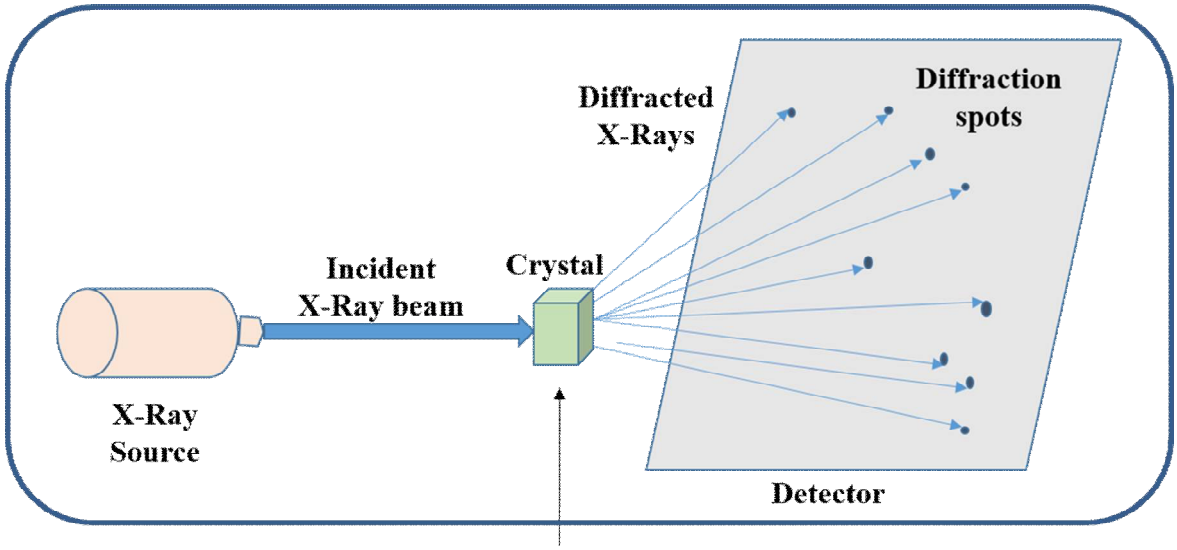

Fig. 3.6 Schematic basic scheme of an X-ray diffraction experiment. An incident X-ray beam enters the crystal and the diffracted rays produce a diffraction pattern (diffraction spots), which are recorded on a detector (Stanjek *et al.*, 2004).

In crystalline structures, the atomic arrays follow an even and repeated pattern. The unit cell is the smallest repeating piece that forms a three-dimensional stacking arrangement. Three axes (*a*, *b*, and *c*) and the angles between them can be used to explain the size and shape of the unit cell in three dimensions (Stanjek *et al.*, 2004). A collection of points arranged periodically in a crystal, known as a lattice, is represented by an array of translation vectors in two and three dimensions. The (hkl) values are known as the Miller indices for a plane or a face, and they can be found by taking the reciprocals of the intersections of the x, y, and z axes in a given lattice plane and finding a perfect integer value for each (Stanjek *et al.*, 2004). The physical interaction of electromagnetic waves with atomic structures of any material produces a diffraction effect only if the wavelength of the incident wave and the periodicity of the crystals are equivalent in magnitude. X-rays are electromagnetic waves with wavelengths of 0.01 to 10 nanometers, similar to the lattice parameters of most crystals. X-rays can be produced by blasting a target (with a high atomic number) with

electromagnetic radiation (enough energy), resulting in the release of an electron from the K-shell. This K-shell electron is filled by electrons from the outer shells (from the L or M shells); the energy difference between these electrons is released as X-rays.

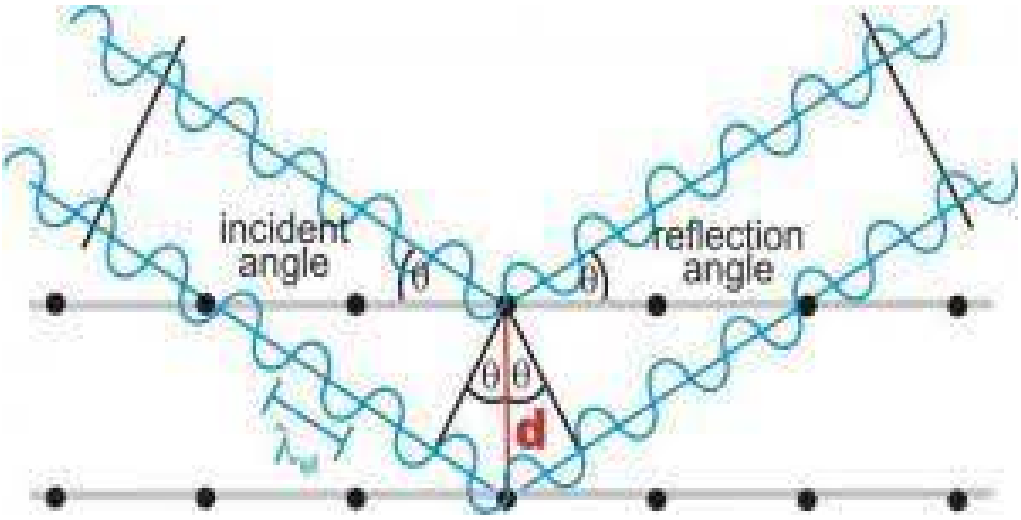

Fig. 3.7 Schematic representation of regularly spaced atomic planes and their interaction with incident X-ray radiations (Stanjek *et al.*, 2004).

When an X-ray interacts with the atomic planes (as illustrated in Fig. 3.7), Bragg's law states that the interference (also known as Bragg reflection) is constructive only when the path difference between the incident and scattered rays is a perfect integer multiple of the wavelength. The Bragg law's requirement for constructive interference must be met by the following equation.

$$n\lambda = 2\ d\ \mathrm{Sin}\ \theta \qquad (3.1)$$

where n is the diffraction order, d represents the inter-planer spacing, θ denotes Bragg's angle measured with respect to the crystal planes, and λ indicates the incident wavelength. In the present research work, the phase formation is identified using the X-ray diffraction pattern obtained using Rigaku Miniflex 600 benchtop diffractometer with Cu-Kα (1.5406 Å) radiation as shown in Fig. 3.8. Cu is used as the target material, and the device is run at 45 kV and 200 mA. A step size of 0.02 (degree) and a count time of 4 seconds are used to record the

data. The software known as Philips X-pert high Score Plus has carried out the phase identification. The XRD analysis is done on the calcined powders, and sintered specimens, and composite powders after SBF immersion.

Fig. 3.8 Rigaku Miniflex 600 benchtop diffractometer.

Additionally, using XRD data, the crystalline phases in the composite sample (3Y-TZP) were calculated. The Garvie and Nicholson technique was used for calculating the molar fraction of monoclinic-ZrO_2, *Xm*, using the relative intensity of monoclinic/tetragonal crystalline peaks existing between 2θ (28-32°) with the help following Equation (3.2) (Habibe *et al.*, 2009).

$$X_m = \frac{I_{m(\bar{1}\,11)} + I_{m(111)}}{I_{m(\bar{1}11)} + I_{m(111)} + I_{t(101)}} \qquad (3.2)$$

Where I_t and I_m indicate the integrated intensity (area under the peaks) of the tetragonal (1 0 1) and monoclinic (1 1 1) and (Γ 1 1) peaks. To compute the monoclinic volume fraction, Vm, use Equation (3.3), as described by Toraya *et al.* (Habibe *et al.*, 2009)

$$V_m = \frac{1.311X_m}{1 + 0.311X_m} \quad (3.3)$$

The tetragonal fraction (V_t) is calculated by the following Equation (3.4),

$$V_t = 1 - V_m \quad (3.4)$$

3.3.3 Fourier transform infrared spectroscopy (FTIR)

Infrared spectroscopy is an important technique for the analysis of materials and provides the fingerprint of the samples investigated in this work. The absorption of FTIR peaks corresponding to the frequencies of vibrations between the bonds of the atom which is responsible for building up the materials (Yadav *et al.*, 2020). Since each material possesses a unique combination of atoms and no two compounds produce the same infrared spectrum. Thus IR spectroscopy can provide identification (qualitative analysis) of different kinds of materials (Titus *et al.*, 2019). A schematic diagram of Fourier transforms infrared (FTIR) spectroscopy is shown in Fig. 3.9. The FTIR is preferred over other infrared spectrum analysis due to the following reasons

- It is a non-destructive technique.
- It provides a precise measurement method that requires no external calibration.
- It can increase the speed of data collection and scan every second.
- It has greater optical throughput.
- It is mechanically simple with only one moving part.

In FTIR, a beam of light of different frequencies interacts with the sample, which excites and vibrates the covalent bonds containing dipole moments, and the detector detects the intensity of light after the interaction. To determine the amount of light absorbed at each wavelength, the interferogram is subjected to a Fourier transform. The data set can be collected in

reflected, absorbed, or transmitted mode. The energy consumed by the bonds is determined by the type of bonds present resulting in a characteristics spectrum (Berthomieu *et al.*, 2009).

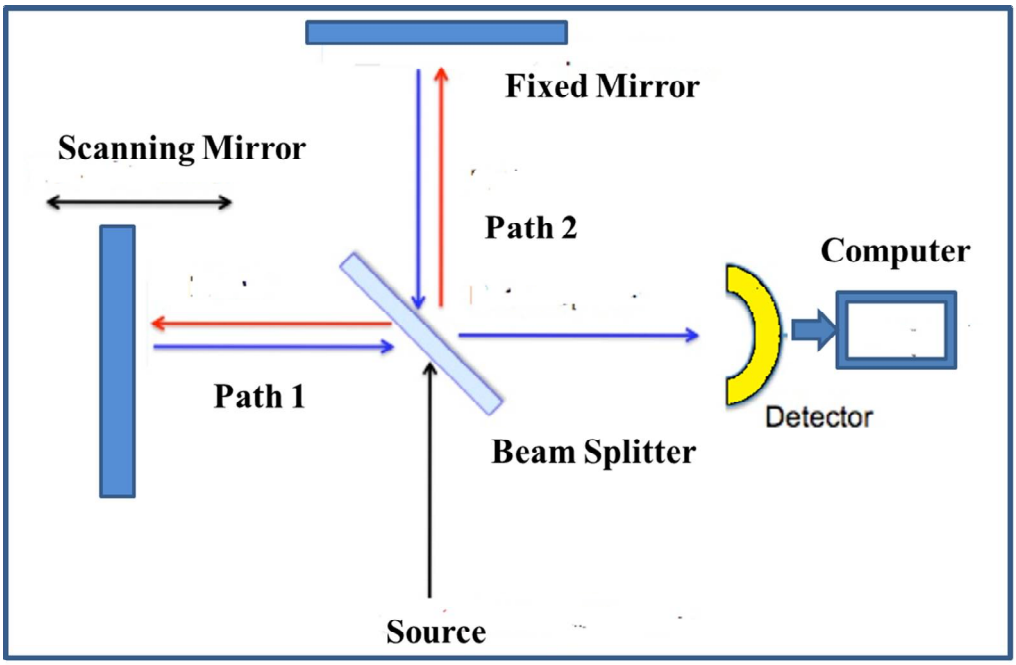

Fig. 3.9 A schematic diagram of Fourier transforms infrared (FTIR) spectroscopy.

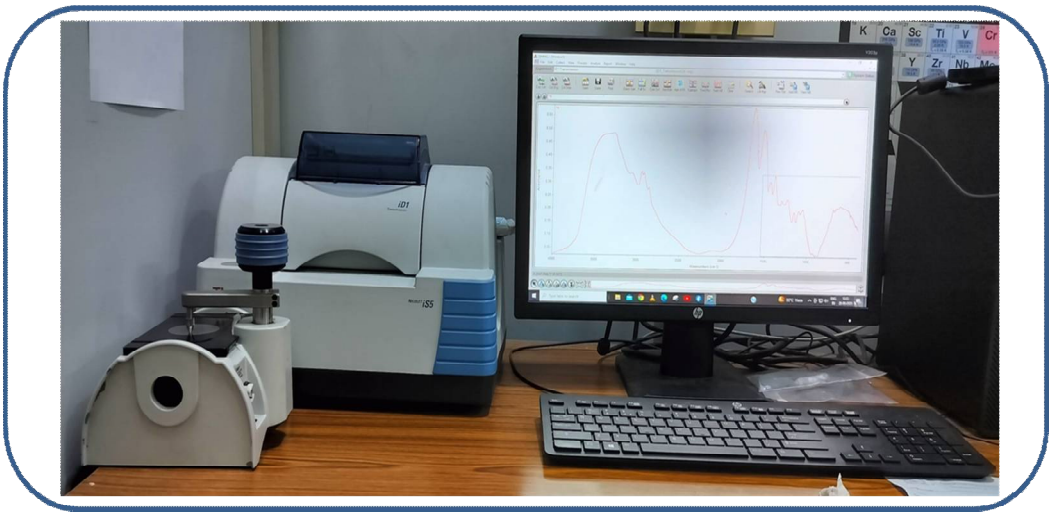

Fig. 3.10 FTIR (BRUKER, TENSOR 27) operating in attenuated total reflectance.

The composite powders in this work were analyzed using FTIR before and after immersion in SBF for bioactivity analysis to see whether any modifications had occurred. All

samples were ground into a fine powder, and spectra were determined at a resolution of 2 cm^{-1} ranging from 400 to 4000 cm-1. Data were collected in transmission mode using an FTIR (BRUKER, TENSOR 27) operating in attenuated total reflectance (ATR) mode, as shown in Fig. 3.10.

3.3.4 Field emission scanning electron microscope (FESEM) with EDS analyser

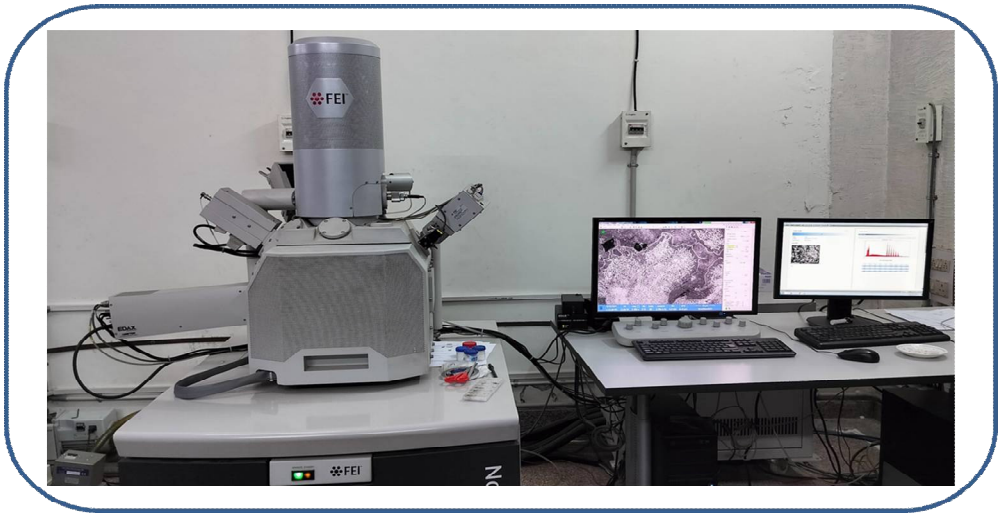

Fig. 3.11 The FE-SEM used in this thesis work has been recorded by EVO18, Zeiss.

A field emission cathode in an electron gun of a scanning electron microscope provides a narrower beam at low as well as high electron energy, resulting in both improved spatial resolution and minimized sample charging and damage (Goldstein *et al.*, 2017). The electrons are generated by a field gradient in the presence of a vacuum, and then the beam passes through electromagnetic lenses and is focused onto the specimen which results generation of various types of electrons through this interaction. A detector ascertains the secondary electron and an image of the surface sample is formed by comparing the intensities of secondary electrons to the primary electron beam. Finally, the image is displayed on a monitor equipped with the FESEM. The FE-SEM images of the investigated samples in this thesis work have been recorded by EVO18, Zeiss, Japan as shown in Fig. 3.11. The FE-SEM

measurement is conducted on the sintered composite specimens, sintered specimens after machining, worm surface of composite samples after wear test, and composite powders after SBF immersion.

The non-destructive energy dispersive X-ray analysis commonly known as EDX or Energy dispersive spectroscopy analysis (EDS) is an X-ray analysis to identify the elemental composition of materials of 0.5 to 1 atomic percent sensitivity. This facility is generally attached with an electron microscopy instrument (SEM, TEM) where a specimen of interest is identified by the impact of a high energy electron beam and ejected electrons from the inner shell of atomic orbitals of elements present in the sample. The resulting vacancy of the inner shell is filled by the electrons available in the shell close to the vacant shell; these transitions are emitted as X-rays. Thus the information corresponding to the elements of the samples can be analyzed on the basis of the energy of the emitted X-ray. EDX gave qualitative, semi-quantitative information about the elements present in the composition. In the present thesis work, the elemental compositions of the prepared samples were confirmed from energy-dispersive X-ray analysis using an EDXA spectrometer as shown in Fig.3.11 attached with FESEM/ EVO18, Zeiss, Japan. This technique was primarily used to detect the elements present in the tested samples and to examine the change in the composition of the composite surfaces after the samples were immersed in SBF.

3.3.5 Density and porosity measurements

3.3.5.1 Bulk density

The bulk density of the sintered composite materials [circular-shaped (OD: 10 mm, Thickness: 2 mm)] was determined by applying Archimedes' principle using Equation (3.5) (Yadav *et al.*, 2020).

$$\text{Bulk density } (\rho_e) = \frac{W_a \times \rho}{W_c - W_d} \qquad (3.5)$$

Where the sample's weights in the air and water are W_c and W_d, respectively, and the density of the water is represented by ρ.

3.3.5.2 Relative density & percentage porosities

Equation (3.6) was used to compute each composition's relative density (RD). Utilizing the rule of mixtures, the theoretical density (ρ_t) of the composite is determined using Equation (3.7). Where ρ_m, v_m, and ρ_r, v_r are the theoretical density, volume fraction of matrix, and reinforcement, respectively. Equation (3.8) is used to compute percentage porosity.

$$\text{RD (\%)} = \left(\frac{\rho_e}{\rho_t}\right) \text{ x } 100 \qquad (3.6)$$

$$\rho_t = \rho_m v_m + \rho_r v_r \qquad (3.7)$$

$$\text{Porosity (\%)} = \left[1 - \left(\frac{\rho_e}{\rho_t}\right)\right] \text{ x } 100 \qquad (3.8)$$

3.3.6 Mechanical properties measurements

3.3.6.1 Flexural strength

The flexural strength of sintered biocomposite materials was performed on a Tinius Olsen H10KL (shown in Fig. 3.12) UTM with a fixed crosshead speed of 0.5 mm/min. For the flexural strength experiment, rectangular bars of 50 mm × 10 mm × 5 mm had been taken (Yadav *et al.*, 2020). Each composition's samples were tested five times, and the final result was derived by taking the average of these. Equation (3.9) was used to calculate the stated values.

$$\sigma_f = \frac{3WL}{2BD^2} \qquad (3.9)$$

Where W is the flexural load, L is the span length, B and D are the width and thickness of the specimen, respectively.

3.3.6.2 Compressive strength

The compressive test of sintered biocomposite materials was performed on a Tinius Olsen H10KL (shown in Fig. 3.12) UTM with a fixed crosshead speed of 0.5 mm/min. A circular specimen with a diameter of 10 mm was used for the compression test. The compressive strength was determined using Equation (3.10) (Pandey *et al.*, 2022).

$$(\sigma_c) = \frac{P}{A} \qquad (3.10)$$

Where P is the compression load, and the area of the sample is denoted by A, where $A = \pi r^2$, the radius of the sample is *r*. The average of the five specimens of each component was used to compute the final outcome.

Fig. 3.12 Universal testing machine (UTM).

3.3.6.3 Hardness

A Vickers hardness machine (Micro hardness Tester LM 248 AT) was used to test the hardness of the sintered biocomposite materials with a diamond indenter. Five indentations

were performed in each sample under a 2000 gf load for a 15-second dwell duration. Equation (3.11) (Soubelet *et al.*, 2018) was used to get the Vicker hardness value.

$$H_v = 1.854 \frac{P}{d^2} \quad (3.11)$$

Where d is the arithmetic mean of the diagonals of the indented region, d_1, and d_2. The H_v was calculated using the mean and standard deviation of 5 indented samples.

3.3.6.4 Elastic moduli

Further**,** an ultrasonic measuring gauge was used to estimate the elastic modulus of the sintered biocomposite samples. The longitudinal (V_L) and transverse wave (V_T) velocities of ultrasonic waves were measured. The polished composite samples were subjected to ultrasonic pulse-echo techniques (45MG, Olympus, USA) to determine the sound wave velocities. The two transducers were used in the test: V116 for the longitudinal wave (10 MHz) and V156 for the transverse wave (5 MHz). Elastic modulus such as longitudinal modulus (L_m), shear modulus (G), bulk modulus (K), Young's modulus (E), and Poisson's ratio (σ) was calculated using the following standard Equations (3.12-3.16) (Issa *et al.*, 2018).

$$L_m = \rho V_L^2 \quad (3.12)$$

$$G = \rho V_T^2 \quad (3.13)$$

$$K = L_m - \frac{4}{3}G \quad (3.14)$$

$$E = \frac{9KG}{3K+G} \quad (3.15)$$

$$\sigma = \frac{E}{2G} - 1 \quad (3.16)$$

3.3.7 Assessment of pH, *in-vitro* bioactivity, and biodegradation measurement

3.3.7.1 pH, and *in-vitro* bioactivity analysis

The *in-vitro* HA forming ability of the developed biomaterials was checked after immersion in SBF solution, which was approved by the International Organization for Standardization. The ionic elements of the SBF are closely similar to those in human plasma, as given in Table 3.4, and can be prepared using the method outlined by Kokubo *et al.* (Yadav *et al.*, 2020). The SBF solution was prepared by adding the proportionate compounds as per Table 3.5.

Table 3.4 Ionic concentration of SBF solution.

	Ionic concentration (mM)							
Ions	Na^+	K^+	Mg^{2+}	Ca^{2+}	Cl^-	HCO_3^-	HPO_4^-	SO_4^{2-}
Simulated body fluid	142.0	5.0	1.5	2.5	147.8	4.2	1.0	0.5
Human blood Plasma	142.0	5.0	1.5	2.5	103.0	27.0	1.0	0.5

Table 3.5 Proportionate weight of compounds to prepare SBF solution.

Order	Reagents	Amount
1.	NaCl	7.996 gm
2.	$NaHCO_3$	0.350 gm
3.	KCL	0.224 gm
4.	$K_2HPO_4.3H_2O$	0.228 gm
5.	$MgCl_2.6H_2O$	0.305 gm
6.	1N HCl	40 ml
7.	$CaCl_2$	0.278 gm
8.	Na_2SO_4	0.071 gm
9.	$NH_2C(CH_2OH)_3$	6.057 gm

The powders of all the samples were placed in polyethylene bottles containing SBF solution (SBF solution: powder - 100:1) for different days at 37ºC. The samples were then taken out from the bottles and kept to dry at room temperature. The *in-vitro* bioactivity of biocomposite powders was analyzed using XRD, FTIR spectroscopy, and SEM. The bioactivity of biocomposite powders was determined by calculating the rate at which the BG transformed into a CaP substance, usually HA. The *in-vitro* formation of a CaP substance indicated the material's bioactive ability in *in-vivo* applications (Silver *et al.*, 2001).

3.3.7.2 Assessment of *in-vitro* biodegradation test

The weight of the glass was lost during the conversion, and the solution's pH was changed. These variations were utilized to track the kinetics of HA formation. For the *in-vitro* degradation study, the disk-type pellets (OD: 10 mm, Thickness: 2 mm) were prepared and sintered, then dipped in the SBF solution for different days. The *in-vitro* degradation was assessed in terms of percentage weight loss by using Equation (3.17) (Yadav *et al.*, 2020).

$$\text{Percentage weight loss } (\%W_L) = \frac{W_{c1} - W_{d1}}{W_{c1}} \qquad (3.17)$$

Where W_{c1} and W_{d1} are the weights of the pellet before and after dipping in SBF, respectively.

3.3.8 *In-vitro* cellular response

For the cellular response of sintered biocomposite samples, MG-63 cells were used and procured from the National Centre for Cell Sciences (NCCS) in Pune, India. The cells were cultured in Dulbecco's Modified Eagle Medium (DMEM) with 15% fetal bovine serum and 1% antibiotic. For the viability (MTT) assay and morphological investigations, the samples were seeded with 10^4 cells per well in a 24-well plate and grown in a CO_2 (5%) incubator at 37ºC.

3.3.8.1 MTT assay

After 3, 5, and 7 days of culture, the viability of the cells on the samples was assessed using the MTT test. After the prescribed period of culture, the growth media was removed from each sample. Thereafter, the samples were washed twice with 1xPBS (phosphate buffer saline). After that, 500 µl MTT solution (MTT: medium ratio - 1:10) was added and put into an incubator for 6 hrs for the formation of the purple formazan crystals. After that, the MTT solution was removed from the well, and DMSO (dimethyl sulphoxide) was added to dissolve the formazan crystals. Subsequently, the optical density (O.D.) of the resulting solution was assessed using an ELISA microplate reader (specifically, the iMark Bio-red model) to determine cell viability. Statistical analyses were performed for multiple comparisons. At a statistical significance level of $p \leq .05$, the ANOVA method (Tukey test) was utilized for statistical analysis of the obtained O.D. Equation (3.18) was used to calculate the percentage of viability of the cells (Yadav *et al.*, 2021).

$$\% \text{ Viability} = \frac{\text{Mean O.D. of sample}}{\text{Mean O.D. of control}} \times 100 \qquad (3.18)$$

3.3.8.2 Fluorescence microscope analyses

The adhesion and morphology of MG-63 cells on the biocomposite samples were observed using a fluorescence microscope (Nikon Eclipse LV 100 ND). After 48 hrs of seeding, the samples were washed with 1xPBS. Afterward, the cells were fixed for 30 minutes in formaldehyde (3.7%). The cells were permeabilized with Triton X-100 and blocked with bovine serum albumin (BSA). The cytoskeletons and nuclei of the adhered cells were stained with Alexa Fluor (488 Phalloidin) and DAPI, respectively.

3.3.8.3 Antibacterial analysis

Antibacterial tests on pure matrix and composite samples were performed with Gram-positive (S. aureus; MTCC 435) and Gram-negative (E. coli; MTCC 443) bacteria. Before sample seeding, both kinds of bacterial cells were cultivated and incubated in Nutrient Agar growth media for 10–12 hrs at 37 °C. After rinsing with 1× PBS, all samples were seeded with bacterial cells of 0.1 O.D. and incubated for 8-10 hrs at 37°C. Following incubation, the samples were rinsed twice with 1×PBS. Then, MTT was incorporated into the cultured samples and incubated for 2 hrs at a ratio of 1:10 with 1×PBS. After the predetermined incubation time, purple-colored formazan crystals were developed, and these were dissolved in DMSO. The mean O.D. was measured with an ELISA microplate reader set to 595 nm wavelengths. The mean O.D. is directly proportional to the viability (living cells) of the bacterial cells.

3.3.8.4 Live/ Dead ratio

The dead cells can be determined by using Equation (3.19)

$$\text{Dead cells (\%)} = 1 - \text{Live cells (viability \%)} \quad (3.19)$$

The Live/ Dead ratio was determined using Equation (3.20)

$$\text{Live/ Dead ratio} = \frac{\text{Live Cells (Viability \%)}}{1 - \text{Live Cells (Viability \%)}} \quad (3.20)$$

3.3.9 Abrasive air jet machining (AAJM)

The AAJM was performed on a mechanical erosion tester machine (model: TR-471-600, Ducom), as shown in Fig. 3.13 (a). The machine was allowed to adjust the erodent flow rate, impingement angle, pressure, velocity, and temperature very precisely. For the machining experiment, rectangular samples of 25 mm × 25 mm × 5 mm were prepared by powder metallurgy route. All prepared samples were sintered at 1250ºC for 4 hrs in a muffle furnace. In AAJM, a mixture of air and erodent particles form a high-pressure jet was struck

on the workpiece surface at particular angles and eroded the materials in the form of small chips and particles. A schematic figure of the MRM is presented in Fig. 3.13 (b). The schematic diagram of the erosion tester setup is shown in Fig. 3.14. Both before and after machining, the samples were cleaned with pressurized air, and the weights were determined using a balance (model: KRT 600, Company KEROY) with a precision of 0.1 mg.

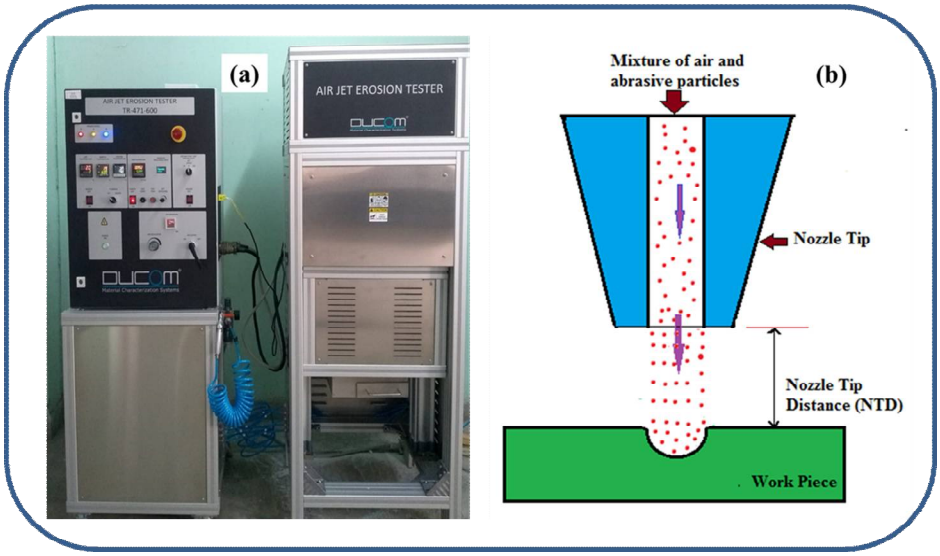

Fig. 3.13 (a) Air jet erosion tester machine and (b) Schematic diagram of material removal mechanics.

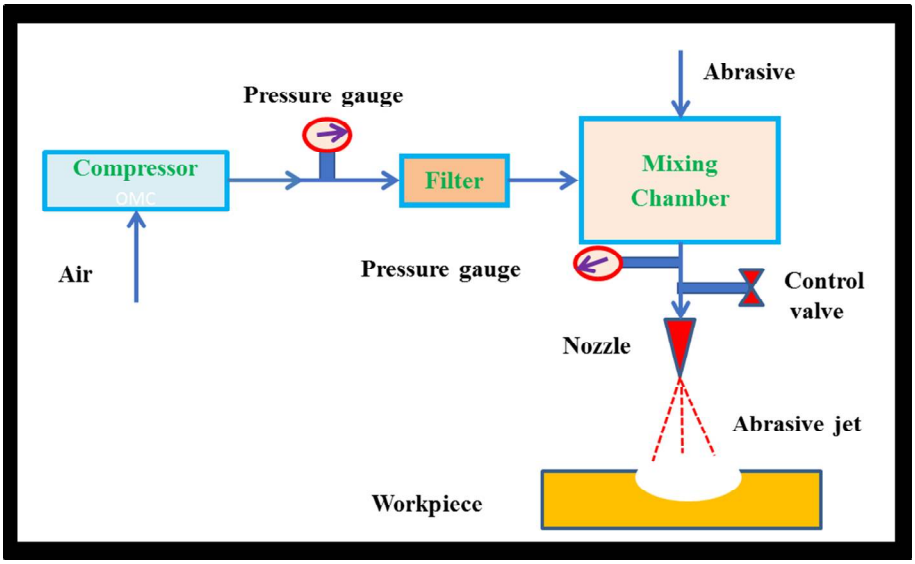

Fig. 3.14 The schematic component-wise diagram of the erosion tester setup.

The process variables that were maintained during the machining are displayed in Table 3.6. Abrasive materials (SiC) were purchased from Otto Chemie Pvt. Limited with 400 mesh size. The morphology of the machined surfaces was analyzed by FE-SEM. Elements presented on the machined surface were conducted by EDX.

Table 3.6 Process parameters during machining.

S. No	Parameters	Conditions
1.	Fluid	Air
2.	Abrasive	Silicon carbide (SiC)
3.	Particle size	400 MESH
4.	Temperature	RT, 200ºC, 400ºC and 600 ºC
5.	Sample size	25 mm × 25mm × 5 mm
6.	Jet discharge rate	3 gm/min
7.	Striking angle	90º
8.	Jet velocity	70 m/s
9.	Pressure	0.45 MPa
10.	Machining time	3 minutes
11.	Nozzle tip distance (NTD)	10 mm
12.	Nozzle diameter	0.6 mm

The machinability behavior of 3Y-TZP/13-93 BG composite materials was studied in terms of MRR (material removal rate) and SR (surface roughness) at ambient and elevated temperatures. The MRR was calculated using Equation (3.21), where the weight difference over the machining period is divided by machining time in minutes (Jagannatha *et al.*, 2021).

$$MRR = \frac{W_1 - W_2}{t} \ gm/min \qquad (3.21)$$

Where W_1 is the weight of the sample before the machining in gm, W_2 is the weight of the sample after the machining in gm, and t is the machining time in a minute. A triplicate test was performed on each composition and took their average for the reported value.

Surface roughness was measured using AFM (model**:** NTEGRA Prima, Company: NT-MDT Service & Logistics Ltd, as shown in Fig. 3.15). All the images were acquired in the scanning region of 10 μm ×10 μm. The topography (within the area: 20 μm × 20 μm) of the tested pellet was analyzed using Atomic Force Microscopy (AFM) (model: NTEGRA Prima, Company). The material removal mechanics (MRM) were also confirmed by the HR-SEM and AFM (atomic force microscopy) analysis.

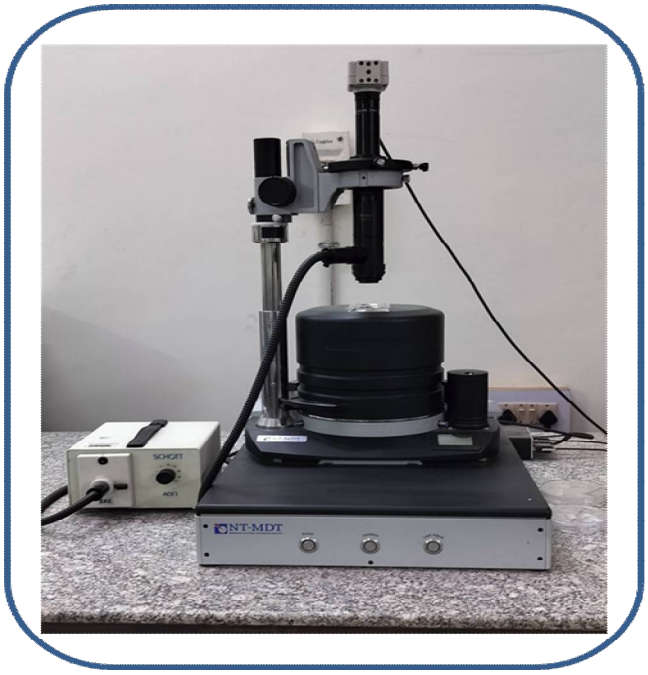

Fig. 3.15 Atomic Force Microscopy (AFM) (model: NTEGRA Prima, Company).

3.3.10 Tribological study

Fig. 3.16 represents the schematic diagram, illustrating the wear test process against to ZrO_2 ball in SBF medium. In wet conditions, sintered 3Y-TZP/13-93 BG composite was subjected to reciprocating wear and friction testing using an automated Bio-tribometer

(Ducom company). In this experiment, a composite sample was stationary, while the counter body was moving. Testing was conducted under wet conditions (SBF solution medium with pH = 7.4) with load to evaluate different scenarios, as they significantly influence the tribological characteristics of samples. Specifically, sintered composite discs of 15 mm diameter, and 4 mm thickness, and counter materials (ZrO_2 balls with a diameter of 10 mm) were utilized for the study. The reciprocating wear track measured 5 mm. A normal load of 20 N was applied to the counter material (ZrO_2 balls). Each test consisted of 1800 cycles at a frequency of 1 Hz, with a sliding distance of 5 mm. The wear track's length was set at 5 mm, which represents the overall stroke length. The width and depth of the wear scar were measured using a contact profilometer (made by Taylor and Hobson in England). First, the wear loss of the worn profile was evaluated using the profilometer then make calculation for the wear loss volume. The average depth was computed using the formula provided by Equation (3.22) (Pandey *et al.*, 2023).

$$D_{avg} = \frac{A_w}{W} \qquad (3.22)$$

Where D_{avg} is the average depth (mm), A_w is the average wear loss area, and W is the average width of each worn scar. Finally, wear volume loss was calculated with the following formula provided by Equation (3.23) (Pandey *et al.*, 2023):

$$\Delta V = [\frac{1}{3} \times \pi \times D_{avg}^2 (3R - D_{avg})] + A_w \times l \qquad (3.23)$$

ΔV, R, and l represent the volume loss (mm^3), zirconia ball radius (mm), and wear track length (5 mm) for each wear track, respectively. The following formula provided by Equation (3.24) was used to calculate the wear rate (W_v) (Pandey *et al.*, 2023):

$$W_v = \frac{\Delta V}{S} \qquad (3.24)$$

Where, W_v denotes the wear rate (mm^3 /min), and S denotes the overall sliding distance (mm). Each experiment was replicated a minimum of three times to ensure consistency and

reliability. Wear rates were determined based on three tracks for each condition. Following the wear test, the sample underwent ultrasonic cleaning in ethanol for 10 minutes. Subsequently, analysis of the worn surface was conducted using optical profilometry, high resolution scanning electron microscopy equipped with energy dispersive x-ray spectroscopy (EDS). After the wear test, another method is used for the calculation of volume loss (ΔV) is a weight loss method. The sample's weight was taken in before and after the wear test using an electronic weight balance, and the weight loss (ΔW) was determined. To calculate volume loss, the formula provided by Equation (3.25) (Kumar *et al.*, 2024) is employed.

$$\Delta V = \frac{\Delta W}{\rho} \qquad (3.25)$$

Where ΔW is weight loss, and ρ is the density of the composites. The machine control unit provided frictional force and computed friction coefficient (μ).

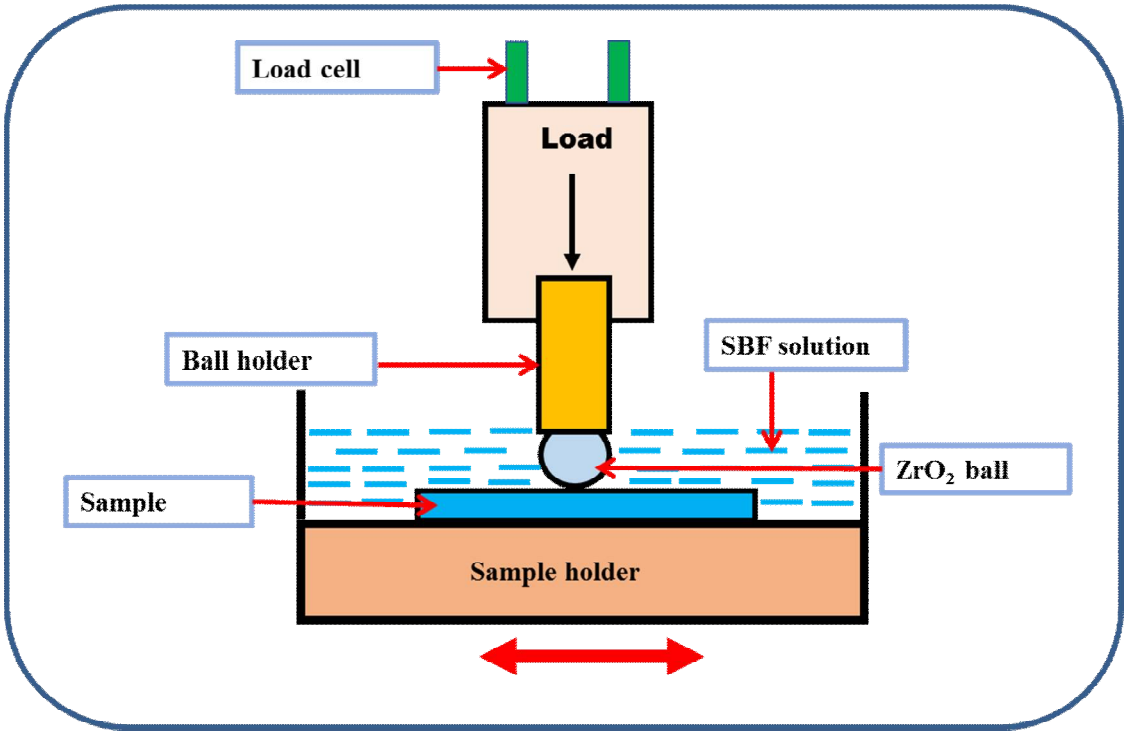

Fig. 3.16 Schematic diagram of wear experiment.